

# Direct observations of fine primary particles from residential coal burning: insights into their morphology, composition, and hygroscopicity

Yinxiao Zhang<sup>1,2</sup>, Qi Yuan<sup>1</sup>, Dao Huang<sup>1</sup>, Shaofei Kong<sup>3</sup>, Jian Zhang<sup>1</sup>, Xinfeng Wang<sup>2</sup>,  
Chunying Lu<sup>2</sup>, Zongbo Shi<sup>4</sup>, Xiaoye Zhang<sup>5</sup>, Yele Sun<sup>6</sup>, Zifa Wang<sup>6</sup>, Longyi Shao<sup>7</sup>, Jihao  
Zhu<sup>8</sup>, Weijun Li<sup>1\*</sup>

<sup>1</sup>Department of Atmospheric Sciences, School of Earth Sciences, Zhejiang University, Hangzhou, Zhejiang, 310027, China

<sup>2</sup>Environment Research Institute, Shandong University, Jinan, Shandong, 250100, China

<sup>3</sup>Department of Atmospheric Sciences, School of Environmental Studies, China University of Geosciences, Wuhan, Hubei, 430074, China

<sup>4</sup>School of Geography, Earth and Environmental Sciences, University of Birmingham, Birmingham, B15 2TT, UK

<sup>5</sup>Key Laboratory of Atmospheric Chemistry of CMA, Institute of Atmospheric Composition, Chinese Academy of Meteorological Sciences, Beijing, 100081, China

<sup>6</sup>State Key Laboratory of Atmospheric Boundary Layer Physics and Atmospheric Chemistry, Institute of Atmospheric Physics, Chinese Academy of Sciences, Beijing, 100029, China

<sup>7</sup>State Key Laboratory of Coal Resources and Safe Mining, China University of Mining and Technology, Beijing, 100086, China

<sup>8</sup>Key Laboratory of Submarine Geoscience, Second Institute of Oceanography, State Oceanic Administration, Hangzhou, 310012, China

\*Corresponding Email: liweijun@zju.edu.cn

## Key points:

- Residential burning of low- and medium-maturity coals emitted abundant carbonaceous particles, while high-maturity coals emitted OM-S.
- Coal maturity and burning temperature substantially affect particulate properties in coal emissions.
- Primary organic and soot particles display extremely weak hygroscopicity and inorganic salts determine hygroscopic growth of mixed particles.

This article has been accepted for publication and undergone full peer review but has not been through the copyediting, typesetting, pagination and proofreading process which may lead to differences between this version and the Version of Record. Please cite this article as doi: 10.1029/2018JD028988

---

## Abstract

Emissions of residential coal burning are an important contributor to air pollution in developing countries, but few studies have yet comprehensively characterized the physicochemical properties of individual primary particles from residential coal burning. Fine primary particles emitted from eight types of coal with low, medium, and high maturity were collected in the flaming and burn-out stages in a typical residential stove. Based on morphology and composition of individual particles, they were divided into six types: organic matter (OM), OM-S, soot-OM, S-rich, metal, and mineral particles. Low-maturity coals (e.g., lignite) dominantly emitted soot-OM particles in the flaming stage; the medium-maturity coals (e.g., medium-maturity bituminous coals) emitted abundant OM particles; and high-maturity coals (e.g., anthracite) emitted abundant OM-S particles. We found that carbonaceous particles from coal burning significantly decreased with an increase of coal maturity; and that soot particles were mainly formed in the flaming stage of low-maturity coals under higher burning temperatures. We concluded that coal maturity and burning temperature both determine particulate properties in coal emissions. In addition, OM and soot particles from residential coal burning displayed extremely weak hygroscopicity, while inorganic salts within individual particles determined particle hygroscopic growth. Understanding the characteristics of particulate matter emitted from residential coal burning is helpful to trace sources of ambient particles and clarify their possible ageing mechanism in air influenced by coal burning emissions. Our results suggest that air quality improvements can benefit substantially from the replacement of low- and medium-maturity coals with high-maturity coals, natural gas or electricity in rural areas.

---

## 1. Introduction

Coal is the second-largest energy source in the world and is expected to increase to 169 quadrillion Btu in 2020 from 153 quadrillion Btu in 2012, related to the quick economic growth of developing countries such as China and India (EIA, 2016). As the biggest consumer of coal in the world, China consumes about 4 billion tons of coal annually, accounting for approximately half of the global coal consumption and more than 60% of the Chinese total primary energy consumption (EIA, 2016; NBSC, 2016). Coal burning can emit large amounts of gaseous pollutants (e.g.,  $\text{SO}_2$ , VOCs) and particulate matter (PM) including organic carbon (OC) and black carbon (BC) (Ge et al., 2004; Zhang et al., 2008), which have additional deleterious effects on human health and global climate (Gohlke et al., 2011; Lacey et al., 2017; Zhang & Smith, 2007). It is estimated that Chinese coal burning emitted 1026 Gg BC and 2335 Gg OC in 2000, contributing 12.8% and 6.9% to global BC and OC emissions from combustion (Bond et al., 2004; Cao et al., 2006). Therefore, at present, China's coal burning has to be considered as a principle source of global anthropogenic carbonaceous emissions.

In rural regions of North China, coal is the dominant fuel for heating and cooking during wintertime (Zhi et al., 2017). It is estimated that residential coal consumption only accounted for 2.2% of total coal consumption, while industrial activities accounted for 94.9% in China in 2014 (NBSC, 2015). However, compared to industrial boilers, coal in residential stoves is incompletely combusted without any air pollution control devices and emits higher volumes of PM (Li et al., 2017a). For example, the emission factors (EFs) of carbonaceous particulate matter from residential stoves are about 100 times higher than that from industrial boilers, even when burning the same coal (Zhang et al., 2008). These features resulted in the contribution of ~35.5% of primary  $\text{PM}_{2.5}$  from residential coal burning to all coal consumption in China in 2010 (Li et al., 2017a). In the Beijing-Tianjin-Hebei region, residential coal burning contributes 46% of the monthly average  $\text{PM}_{2.5}$  concentration (Zhang et al., 2017b). Recent studies suggest that primary emissions from residential coal burning significantly contribute to the formation of Chinese haze during wintertime (Chen et al., 2017; Li et al., 2018; Liu et al., 2016). Therefore, it is necessary to study the characteristics of

---

primary particles from residential coal burning.

Various bulk technologies have been used to obtain mass concentrations and compositions of primary particles from residential coal burning, including OC, elemental carbon (EC), inorganic ions, and polycyclic aromatic hydrocarbons (PAHs) (Chen et al., 2005; Shen et al., 2010; Zhang et al., 2008). However, they cannot provide detailed information on morphology, composition, and mixing state of individual primary particles, which is crucial to study their ageing and reaction processes in the atmosphere, and then further to clarify the mechanisms of Chinese haze formation in the winter (Li et al., 2016). To our knowledge, few studies on the comprehensive features of individual primary particles directly derived from coal burning have been reported.

In this study, eight types of raw coal with a wide range of maturity were selected from North China and burned in a typical residential stove. The fine primary particles were collected during the flaming and burn-out stages, and then analyzed with transmission electron microscopy (TEM). Our aim was to establish an empirical basis that included the morphology, composition, and mixing state of primary particles from the combustion of different types of coal. Moreover, hygroscopic properties, OC, EC, and soluble inorganic ions of primary particles from residential coal burning were also investigated.

## **2. Experiments**

### **2.1. Coals and sampling system**

Detailed information on eight types of raw coal is summarized in Table 1. These typical coals were collected from different main coal-mining regions in North China, and they covered a wide range of maturity with vitrinite reflectance ( $R_o$ ) varying from 0.33% to 7.38%, including a lignite from Inner Mongolia (IM/LI); five bituminous coals: a gas coal from Shaanxi (SN/GC), two non-caking coals from Shaanxi (SN/NC) and Inner Mongolia (IM/NC), a fat coal from Shandong (SD/FC), a meager coal from Shanxi (SX/MC); an anthracite from Shanxi (SX/AN), and a natural coke from Shanxi (SX/NCC).

A typical residential stove that is made of cast iron and widely used to burn raw coal chunks for heating and cooking in rural regions of North China was used in our experiment. The sampling system was composed of four parts: residential stove, dilution tunnel,

---

suspension chamber, and sampling part (Figure S1). Details of the sampling system have been described by Liu et al. (2017).

## 2.2. Sampling

Large raw coal chunks were broken into small pieces, and some of them were ignited outside the stove. We moved these burnt coals into the bottom chamber of the residential stove and then added more fresh coals onto the burnt coals. In this study, coals were burnt in the stove without any control of oxygen supply and burning temperature to simulate the actual coal combustion in rural regions. In order to know the emission characteristics of different burning stages, coal burning was divided into two stages: a flaming stage when coal was burning with flames, and a burn-out stage when coal was burning out without flames (Figure S1). Because coals naturally burned in the stove without any control, raw coals with and without flames occurred during the flaming stage. The flaming stage in this study reflects the mixture of ignition, fierce combustion, and relatively stable combustion of coals under the precise controls described by Zhou et al. (2016). Before we collected aerosol particles, the dilution tunnel and suspension chamber were cleaned thoroughly for 15 min by the blower with a pre-filter. When coal burning reached the flaming or burn-out stage, the pump connected to the chamber was switched on after two valves were opened, and part of the smoke from the coal burning entered into the chamber of 1 m<sup>3</sup> through the dilution tunnel. The smoke was diluted about 20–25 times with particle-free air and cooled down at about 25°C in suspension chamber before we collected particles. The details of temperatures of the two burning stages of each coal are listed in Table S1.

Individual primary particles were collected on copper TEM grids covered by carbon film (carbon type-B, 300-mesh copper; Tianld Co., China) using a single-stage cascade impactor (jet nozzle diameter: 0.5 mm, air flow rate: 1.0 L·min<sup>-1</sup>) in the flaming and burn-out stages. The individual particle sampler has a collection efficiency of 50% at 80 nm aerodynamic diameter if the density of the particles is 2 g·cm<sup>-3</sup>. To collect the fine particles, we installed one pre-filter with a polycarbonate membrane (Whatman, UK) with 2 µm pores before the particles were pumped into the single particle impactor. Therefore, those fine particles with diameter < 2 µm were only collected in the fresh smoke plume. After aerosol collection, the TEM grids were stored in a sealed, dry plastic container. We used 47 mm quartz filters to

---

collect PM<sub>2.5</sub> using a pump with a flow rate of 10 L·min<sup>-1</sup> during the flaming stage. After sampling, quartz filters were stored in a refrigerator for later analyses. More information about these samples can be found in Table S1.

### 2.3. Analyses

Quartz filters were analyzed by a Sunset OC/EC analyzer (Sunset Lab, USA) for OC and EC, and by ion chromatography (Dionex ICs-90, USA) for water-soluble inorganic ions (i.e., Na<sup>+</sup>, NH<sub>4</sub><sup>+</sup>, K<sup>+</sup>, Mg<sup>2+</sup>, Ca<sup>2+</sup>, Cl<sup>-</sup>, SO<sub>4</sub><sup>2-</sup>, and NO<sub>3</sub><sup>-</sup>). More detailed information about these analyses is provided in Zhang et al. (2017a).

Individual primary particles collected on TEM grids were analyzed by a JEOL JEM-2100 TEM operated at 200 kV. Elemental composition was determined semi-quantitatively by an energy-dispersive X-ray spectrometer (EDS) that can detect elements heavier than carbon (C). EDS analyses show that the C content of carbonaceous particles was much higher than that of the carbon film (Figure 1b). Copper was excluded from the analysis because the TEM grids were made of copper. The distribution of aerosol particles on TEM grids was not uniform, with coarser particles occurring near the center and finer particles occurring on the periphery. Therefore, to ensure that the analyzed particles were representative, three or four areas were chosen from the center to periphery of each grid. The projected areas of individual particles were determined using iTEM software (Olympus Soft Imaging Solutions GmbH, Germany), the standard image analysis platform for electron microscopy.

On the basis of TEM analysis, one typical sample was chosen for ion analysis using the NanoSIMS 50L (Institute of Geology and Geophysics, Chinese Academy of Sciences). In this study, <sup>12</sup>C<sup>14</sup>N<sup>-</sup>, <sup>12</sup>C<sup>-</sup>, <sup>16</sup>O<sup>-</sup>, and <sup>32</sup>S<sup>-</sup> ions in individual particles were obtained, when the Cs<sup>+</sup> primary ion beam caused the ionization of atoms within the particles. Furthermore, ion intensity mappings with nanometer resolution displayed the distribution of different ions in individual particles. In this case, <sup>12</sup>C<sup>14</sup>N<sup>-</sup> and <sup>12</sup>C<sup>-</sup> ions represented the organic matter (OM) in individual particles, and excluded the contribution from the carbon substrate (Chi et al., 2015; Li et al., 2017b).

Scanning electron microscopy (SEM) (Zeiss Ultra 55) was also used to gain detailed information on surfaces of individual aerosol particles. This type of electron microscope can

---

obtain particle surface information by scanning it with a high-energy beam of electrons in a raster scan pattern. To obtain vertical or depth information on individual particles, we tilted the sample stage at a 55° angle and then took particle images.

#### **2.4. Hygroscopic experiment**

An individual particle hygroscopic (IPH) system was built to observe the hygroscopic properties of individual primary particles at different relative humidity (RH). The IPH system involved three steps: (1) introducing N<sub>2</sub> gas with a mass flow controller into a chamber; (2) setting a TEM grid or silicon wafer on the bottom of an environmental microscopic cell (Gen-RH Mcell, UK), which can change RH and keep temperature at 20°C; and (3) taking images at incremental RH values using an optical microscope (Olympus BX51M, Japan) with a camera (Canon 650D). This IPH system has successfully captured the hygroscopic growth of individual particles collected on either a silicon wafer or TEM grid (Chi et al., 2015; Li et al., 2014; Sun et al., 2018). In this study, four typical samples were chosen to observe hygroscopic growth of OM, OM-S, and soot-OM particles at RH values ranging from 5% to 94%. The particle growth factor (GF) is an important parameter used to describe the hygroscopic growth of individual particles, which is defined as:

$$GF(RH) = \frac{D(RH)}{D_0}$$

where  $D(RH)$  and  $D_0$  are the diameters of particles at a given RH and at 5% RH, respectively.

### **3. Results and Discussion**

#### **3.1. Main types of individual primary particles**

1968 primary particles from residential coal burning were detected by TEM with particle sizes from 40 nm to 4.5 μm. Particles displayed a broad peak from 350 nm to 550 nm by the equivalent circle diameter (Figure S2). Based on the elemental composition of fine primary particles, we found most particles contained C and minor O and Si (Figures 1a–c, 2a, and 2c). To address the interference of the carbon film on EDS analyses carried out on the TEM grid, the NanoSIMS was adopted to verify one typical spherical carbonaceous particle through <sup>12</sup>C<sup>14</sup>N<sup>-</sup> and <sup>12</sup>C<sup>-</sup> mapping (Figure 1e–h). The typical carbonaceous particle displayed strong <sup>12</sup>C<sup>14</sup>N<sup>-</sup> and <sup>12</sup>C<sup>-</sup> signals, but a weak <sup>32</sup>S<sup>-</sup> signal. As a result, we determined that this type of

---

carbonaceous particle was OM. In addition, we easily identified soot particles because of their chain-like aggregation morphology in the samples (Figure 1c). The high-resolution TEM image clearly displays that these soot particles contain graphitic layers with an onion-like structure (Figure 1d). In this way, morphology was confirmed to differentiate between OM and soot particles.

To characterize the fine primary particles emitted from residential coal burning, we classified them into six particle types based on their morphology and composition: OM (Figure 2a), OM-S (Figure 2b), soot-OM (Figure 2c), S-rich (Figure 2d), metal (Figure 2e), and mineral (Figure 2f). Detailed information about the classification of individual particles has been described in Li et al. (2016) and Pósfai et al. (2003).

The primary OM particles were stable under the strong electron beam and contained C, O, and Si with minor amounts of S and Cl (Figure 2a). Based on their different morphologies, OM particles were further divided into three types: spherical OM (Figure 2a-1), dome-like OM (Figure 2a-2), and irregular OM (Figure 2a-3). The SEM image taken at sample stage tilted 55° angle clearly shows that the spherical OM particles are solid balls, given their vertical dimensions (Figure 1i). Morphology and composition of spherical OM particles are similar to tar balls emitted from biomass burning (Chakrabarty et al., 2010; Hand et al., 2005; Pósfai et al., 2004). Adachi and Buseck (2011) suggested that droplet-like OM from biomass burning can solidify and form tar balls during the ageing of smoke plume. Furthermore, the SEM image shown in Figure 1j shows that abundant dome-like OM particles on the substrate are rather flat, suggesting that these particles are liquid phase or mixtures of solid and liquid phases before collection. Based on dehydration and oligomerization of low-volatility organic compounds in hydrated particles proposed by Pósfai et al. (2004), these dome-like OM are expected to become spherical OM as they age (Tóth et al., 2014). Therefore, spherical OM particles that resemble tar balls are typical refractory organic particles.

Soot particles, also named as BC and EC, are aggregates of carbonaceous spheres with diameters from 10 to 100 nm. Soot particles mainly consist of C and minor O and Si (Figure 2c). In this study, soot particles displayed two forms: chain-like soot (Figure 2c-1) and cluster-like soot (Figure 2c-2), most of which were internally mixed with OM. Therefore, we use soot-OM to represent these particles.

---

S-containing particles were sensitive to the strong electron beam of TEM and were easily sublimated. According to their sulfur content measured using the EDS, particles with sulfur > 60% were named as S-rich particles (Figure 2d), while other S-containing particles were assigned to OM-S particles, which contained abundant C and certain amounts of S, and minor Cl (Figure 2b).

Only a few metal and mineral particles were observed in the samples. For example, a Fe-rich particle exhibited a spherical shape (Figure 2e) while a Ca-rich mineral particle was irregular (Figure 2f).

### **3.2. Primary particles from lignite burning**

Lignite has a low degree of coalification and contains high amounts of volatile substances. Zhang et al. (2011) estimated that the reserves of lignite are about 130 billion tons in China, most of which are in Northeast China, especially in eastern Inner Mongolia. Therefore, lignite from Inner Mongolia (IM/LI) was chosen for this experimental work and was burned in the residential stove to reveal the emission characteristics of its individual primary particles.

*IM/LI.* In the flaming stage, we found that cluster-like soot particles with OM coating accounted for 79% of the total number of analyzed particles (Figure 3a-1, 3a-2 and Table 2) and OM particles accounted for 21% (Table 2). These OM particles mainly included spherical OM (Figure 3a-3) and their aggregations (Figure 3a-4). In the burn-out stage, the dominant primary particles became OM particles, accounting for 74% of all analyzed particles (Table 2). Interestingly, TEM observations show that most OM particles were dome-like OM, and some of them had dark OM inclusions (Figure 3a-5, 3a-6). In addition, 18% of primary particles were OM-S particles (Figure 3a-8 and Table 2), but only 8% were soot-OM particles (Figure 3a-9 and Table 2). Compared to the flaming stage, the fraction of soot-OM particles decreased from 79% to 8%, while OM and OM-S particles increased from 21% to 92% in the burn-out stage (Table 2).

### **3.3. Primary particles from bituminous coal burning**

Bituminous coals with a moderate degree of coalification have a wide distribution and abundant production throughout China. According to the China Coal Industry Yearbook, the production of bituminous coal was 2.1 billion tons in 2008, accounting for 77% of total coal

---

production. Because of its high production and low cost, bituminous coal has been the most widely used material in residential stoves in rural China. Previous studies suggested that residential bituminous coal burning has higher EFs of PM, OC, EC and PAHs than anthracite, and it has become a main contributor to Chinese air pollution (Chen et al., 2005; Chen et al., 2006b; Liu et al., 2009). In this study, we collected five bituminous coals, including one with low maturity (SN/GC), three with medium maturity (SN/NC, IM/NC, SD/FC), and one with high maturity (SX/MC).

**SN/GC.** TEM observations show that all the primary particles were chain-like soot-OM particles in the flaming stage (Figure 4a-1 and Table 2). Figure 4a-2 clearly shows that the chain-like soot particles were coated by OM, so we could not distinguish the primary spherules in the soot particles. In the burn-out stage, we found that 77% of primary particles were soot-OM particles (Table 2). Moreover, some soot particles were attached to OM (Figure 4a-3). Compared to the flaming stage, more external OM particles occurred in the burn-out stage (Figure 4a-4), accounting for 23% of total primary particles (Table 2).

**SN/NC.** TEM observations show that 98% of primary particles were OM, while only 2% were soot-OM particles in the flaming stage (Table 2). Figure 4b-1 and 4b-2 show that most OM particles were dome-like OM and some of them had dark spherical OM inclusions. In the burn-out stage, all the particles were dome-like OM (Figure 4b-3, 4b-4 and Table 2). Interestingly, 16% of dome-like OM were internally mixed with tiny soot particles (named as OM-soot) (Figure 4b-4 and Table 2).

**IM/NC.** In the flaming stage, all the primary particles were OM particles, including abundant spherical OM and small amounts of irregular OM (Figure 4c-1, Figure 4c-2 and Table 2). Figure 4c-1 shows that a low-magnification TEM image contained 11 OM particles, ten of which were the spherical OM or their aggregations. In the burn-out stage, all the primary particles became dome-like OM and some of them had the dark OM inclusion (Figure 4c-3, 4c-4 and Table 2). This result was similar to those for the burn-out stages of IM/LI and SN/NC samples.

**SD/FC.** TEM observations show that 77% of primary particles were OM particles and 23% were soot particles partly mixed with OM in the flaming stage (Figure 4d-2 and Table 2). OM particles occurred as three different types: spherical OM, dome-like OM, and irregular

---

OM (Figure 4d-1, 4d-2). In the burn-out stage, the primary particles were similar to OM particles in the flaming stage (Figure 4d-3, 4d-4).

*SX/MC*. Meager coal has the highest degree of coalification of all bituminous coals. In this study, the vitrinite reflectance of meager coal was 1.98% (Table 1), which is close to that of anthracite. TEM observations show that all the primary particles in the flaming and burn-out stages were OM-S particles (Figure 4e and Table 2). Figure 4e-1 clearly exhibits that OM particles were internally mixed with sulfate in the flaming stage. Under the strong electron beam, sulfate particles were damaged and OM residues were left on the substrate (Figure 4e-2). In the burn-out stage, most OM-S particles were also sensitive under the strong electron beam, but presented as chain-like shapes (Figure 4e-3 and 4e-4).

### **3.4. Primary particles from anthracite and natural coke burning**

*SX/AN*. Anthracite contains a high degree of fixed carbon and a low amount of volatiles. According to the Chinese classification of coals (GB/T 5751-2009), the volatile contents on dry and ash-free basis of anthracite is less than or equal to 10%. Compared to bituminous coal and lignite as shown above, we observed that anthracite combustion emitted lighter smoke and it is a better fuel for heating and cooking in winter. However, anthracite is less popular than bituminous coals in rural regions because of its higher price. Here we selected one anthracite from Shanxi province (*SX/AN*). TEM observations show that all the primary particles in the flaming stage were OM-S (Table 2). Interestingly, these OM-S particles were aggregations of several near-spherical OM particles internally mixed with sulfate (Figure 5a-1, 5a-2). In the burn-out stage, we only collected a few particles on the substrate because of light smoke. These primary particles were OM (21%), OM-S (27%), S-rich particles (18%), and mineral particles (34%) (Table 2).

*SX/NCC*. Natural coke is coal altered by the relatively local elevated heat flow caused by an intrusive body (Kwiecinska & Petersen, 2004). This coal with its high ignition point is seldom used as a residential fuel. Due to its complex formation process, natural coke can be mixed with other coals like anthracite. Here we collected one natural coke with the highest vitrinite reflectance of 7.38% from Shanxi province (*SX/NCC*) (Table 1). TEM observations show that 80% of primary particles were OM-S in the flaming stage (Table 2). These OM-S particles were aggregations of several near-spherical OM-S particles and appeared as soot

---

chain-like shapes (Figure 5b-1). However, these particles were sensitive under the electron beam and completely different from the stable chain-like soot particles on the substrate. Also, we detected metal particles (like spherical Fe in Figure 5b-2) and mineral particles (Figure 5b-3) mixed with OM-S particles. These metal-containing and mineral particles accounted for 13% and 7% of total primary particles, respectively (Table 2). In the burn-out stage, we notice that 82% of primary particles were OM-S, which was similar to those in the flaming stage, and 18% were S-rich particles (Figure 5b-4, 5b-5 and Table 2).

### **3.5. Effects of coal maturity and burning temperature on the emissions**

Figure 6 shows the various types of coal and their relative abundances of six individual particle types from the flaming and burn-out stages as well as the relative abundances of OC, EC, and soluble inorganic ions in PM<sub>2.5</sub> emitted during the flaming stage. The low-maturity coals (e.g., IM/LI and SN/GC) normally emitted more soot-OM particles in the flaming stage compared to other coals (Figure 6a). Especially in the case of SN/GC, all the primary particles emitted from the flaming stage were soot-OM particles (Figure 6a). This result is consistent with the bulk analyses that show low-maturity coals with higher mass fractions of EC, and that sample SN/GC had the highest mass fraction of EC in the flaming stage compared to other coals (Figure 6b). Moreover, certain amounts of OC were also detected in PM<sub>2.5</sub> samples from low-maturity coals. These results suggest that soot particles from low-maturity coals were indeed mixed with OM, as shown in Figures 3a (-1, -2) and 4a.

Individual primary particles from bituminous coals with medium maturity, including SN/NC, IM/NC and SD/FC, were dominated by OM particles, while only a few OM particles were associated with soot particles (Figures 4b–d and 6a). Similarly, the bulk analyses show that the mass fractions of OC from these three coals were higher than 70% among OC, EC and ions (Figure 6b). Therefore, the medium-maturity bituminous coals emitted large amounts of OM particles. Previous studies have obtained similar results. For example, Chen et al. (2006b) reported that the average OM/PM value was 66% for five bituminous coals with R<sub>o</sub> ranging from 0.58% to 1.00% burned in a residential stove; Zhi et al. (2008) found that the average mass contribution of OM to PM was more than 80% for five bituminous coals with medium-maturity although they were burned in the form of honeycomb briquettes. These comparisons indicate that the microscopic analysis of individual particles does reflect

---

the emission properties of residential coal burning.

Individual primary particles from the high-maturity coals, including SX/MC, SX/AN, and SX/NCC, were mainly a mixture of OM and sulfate. Figure 6b shows that soluble inorganic ions from the high-maturity coals had higher mass fractions of PM<sub>2.5</sub> than those from low- or medium-maturity coals in the flaming stage. We noticed that SX/NCC emitted the highest mass fraction of soluble inorganic ions in the flaming stage among all coals (Figure 6b). This result is consistent with the high number fractions of OM-S particles in individual particle samples (Figures 5b and 6a). TEM observations and bulk results both reveal that the high-maturity coals emitted less carbonaceous particles and more inorganic aerosol components. This result is similar to the study of Huang et al. (2014b), in which the mass fractions of N and S in PM emitted from high-maturity coal (R<sub>o</sub> is 1.88%) were much higher than those from low- and medium-maturity coals, while the mass fraction of C was much lower. Zhou et al. (2016) also found that ammonium, sulfate, and chloride were the dominant components in the flaming stage of residential anthracite burning.

To summarize, under residential burning conditions, the low- and medium-maturity coals emitted high-density black smoke with abundant carbonaceous particles, while the high-maturity coals produced lighter smoke with a mixture of carbonaceous and inorganic species. Our results point to the general conclusion that coal maturity significantly influences emissions from residential coal burning. This is generally consistent with previous studies (Chen et al., 2009; Huang et al., 2014c; Wang et al., 2016; Zhi et al., 2008). For example, Chen et al. (2009) indicated that EFs of carbonaceous particles from bituminous coals are 1 to 3 orders of magnitude higher than those from anthracite. Huang et al. (2014c) reported that residential anthracite burning in honeycomb briquettes yielded PAHs concentrations that were 10–100 times lower than bituminous coals. As indicated in these studies, coal maturity largely determined the mass and types of residential particle emissions.

Carbonaceous particles from the low-maturity coals contained higher amounts of soot-OM particles. For example, all primary particles from the flaming stage of SN/GC were chain-like soot-OM particles, whereas other types of bituminous coals rarely emitted soot particles (Figures 4 and 6a). We noticed that the burning temperature of SN/GC was close to 1000°C in the flaming stage, which is much higher than 783–943°C of other bituminous coals

---

(Table S1). Moreover, more soot particles were formed in the flaming stage than in the burn-out stage (Figure 6a). This result was generally attributed to the higher temperatures in the flaming stage than in the burn-out stage (Table S1). Low temperature can inhibit graphitization and the formation of soot (Bond et al., 2002). As a result, the temperature of coal burning has an important influence on the formation of soot in addition to the coal maturity.

### **3.6. Hygroscopic properties of primary particles**

In this study, we also observed the hygroscopic properties of three main types of particles (i.e., OM, soot-OM, and OM-S), based on the results shown in Figure 6. Figure 7 shows that OM and soot-OM particles only displayed small growth factors of 1.014 and 1.015 at 94% RH, respectively, suggesting that the primary OM and soot particles have extremely weak hygroscopicity. However, all the OM-S particles with different sizes on the substrate displayed a dramatic size growth at 68–85% RH (Figure 7). These results are similar to the study by Semeniuk et al. (2007), in which they found that soot and tar balls from biomass fires were hydrophobic while the mixed organic-inorganic particles took up water between 55 and 100% RH. Interestingly, we found that individual particles containing minor inorganic salts can completely change the hygroscopicity of soot and OM particles (Figure 7c). The hygroscopicity of aerosol particles is dependent on their chemical compositions (Jing et al., 2016; Sun et al., 2018). TEM/EDS results show that many OM-S particles emitted from different coals commonly contained small amounts of inorganic sulfate salts or a mixture of sulfates and chlorides (Figures 2–5), which was consistent with the bulk analysis of PM<sub>2.5</sub> containing minor various soluble ions (known as secondary inorganic particles) by mass compared with EC and OC (Figures 6b, S3). This result can be understood by realizing that chemical variations of inorganic salts in the OM-S particles from different samples probably induce different hygroscopic growth throughout the range of RH (68–85%). As a result, these inorganic species significantly determine the hygroscopicity of primary OM and soot particles from residential coal burning.

## **4. Conclusions and atmospheric implications**

In this study, primary particles emitted from eight types of coal with different maturity

---

were collected in the flaming and burn-out stages in a typical residential stove. According to the morphology and composition of individual particles using TEM/EDS, we classified six main types: OM, OM-S, soot-OM, S-rich, metal, and mineral particles. Based on the results in this study, we developed a conceptual model to summarize how coal maturity and burning conditions in the stoves influence particulate emissions (Figure 8). In the flaming stage, the low-maturity coals emitted much higher BC (i.e., soot) particles than the medium- and high-maturity coals, while TEM observations reveal that these soot particles exhibited cluster-like or chain-like shapes and were internally mixed with OM. In emissions from the medium-maturity coals, OM particles, such as spherical OM, dome-like OM and irregular OM, were the dominant particles, and relative mass fractions of OM reached a peak. However, in emissions from the high-maturity coals, the dominant particles were a mixture of OM and sulfate (OM-S). In other words, the low- and medium-maturity coals emitted more carbonaceous particles, while the high-maturity coals emitted a mixture of carbonaceous and inorganic species. In addition, we found soot particles were mainly produced under high burning temperatures in the flaming stage of burning low-maturity coals. Therefore, coal maturity and burning temperature strongly influence the characteristics of coal emissions and particle formation. Hygroscopic experimental analysis revealed that OM and soot particles from residential coal burning have extremely weak hygroscopicity and that inorganic salts internally mixed with carbonaceous species determine the hygroscopic growth of these particles.

Residential coal burning, particularly of IM/NC and SD/FC, can emit abundant spherical OM particles (Figure 4c and 4d). Compared to tar balls from biomass burning, some studies indicated that spherical OM particles from coal burning generally contain much higher Si (Chen et al., 2017; Li et al., 2012; Zhang et al., 2017a). It is still unknown whether spherical organic particles from coal and biomass burning have similar organic compounds and optical absorption. Here, we have determined that these spherical OM particles from coal burning are refractory organics, which likely contain PAHs and humic-like substances (Andreae & Gelencsér, 2006). Therefore, we expect that these spherical OM particles are light-absorbing aerosols and belong to the family of atmospheric brown carbon (BrC), as described in the previous studies (Alexander et al., 2008; Hoffer et al., 2016).

---

Soot particles were mainly emitted from low-maturity coals burning. Compared to the bare, chain-like soot particles from vehicular emissions, we could not clearly see carbonaceous monomers in many soot particles from coal burning because of their OM coatings (Figure S4). Therefore, the soot particles from residential coal burning contain not only black carbon, but also considerable amounts of organic carbon. The difference in optical absorption of soot particles from coal burning and vehicles remains unclear and is ripe for further investigation.

OM-S and S-rich particles, which are known to be formed through atmospheric oxidation of gaseous  $\text{SO}_2$  emitted from coal burning, are commonly referred to as secondary sulfate aerosols (Huang et al., 2014a). In this study, we found that residential coal burning can also directly emit some OM-S particles and S-rich particles (Figures 4e, 5a and 5b). Ionic analyses of  $\text{PM}_{2.5}$  samples revealed that  $\text{SO}_4^{2-}$  was dominant in the soluble inorganic ions (Figure S3). From this work, we conclude that sulfates in the ambient air must include the contribution of primary emissions from residential coal burning.

$\text{Cl}^-$  was another major soluble inorganic ion in  $\text{PM}_{2.5}$  from residential coal burning (Figure S3). TEM/EDS analyses also detected certain amounts of elemental chlorine in both OM and OM-S particles (Figure 2a, 2b). This explains why chlorine is much higher in  $\text{PM}_{2.5}$  during wintertime than summertime in North China (Sun et al., 2013). Ionic analysis indicates that  $\text{Cl}^-$  could be related to  $\text{NH}_4^+$ , which is decidedly different from the KCl from biomass burning (Liu et al., 2017; Reid et al., 2005). In summary, residential coal burning is an important source of chlorine in winter in North China.

Burning of low- and medium-maturity coals can emit abundant carbonaceous particles, including primary OM and soot particles, which are dominant fine particles and contribute to wintertime haze formation in North China (Chen et al., 2017; Liu et al., 2016; Sun et al., 2013; Zhang et al., 2017a). For example, Zhang et al. (2017a) found that the enrichment of primary OM from residential coal burning can cause the light and moderate wintertime haze formation in Northeast China. Moreover, primary carbonaceous particles from residential coal burning tend to be smaller than  $1 \mu\text{m}$  (Figure S2) and contain abundant toxic compounds, such as PAHs (Kong et al., 2018; Liu et al., 2009; Zhang et al., 2008). Once these particles are emitted from residential coal burning into indoor or ambient air, they can easily be

---

deposited deep into the lungs and consequently these particles are extremely harmful to human respiratory health (Lighty et al., 2000). The mass of fine primary particles from residential coal burning depends somewhat on the burning stages, but is mostly determined by coal maturity. Compared to low- and medium-maturity coals, combustion of high-maturity coals emits much less smoke with fewer OM and soot particles, which might have less adverse effects on air quality and human health. Therefore, high-maturity coals are a better choice of fuel for residential heating and cooking than low- and medium-maturity coals. In addition, replacing coal as the heating and cooking fuel with natural gas and electricity is also an efficient way to mitigate air pollutants and improve air quality (Chen et al., 2006a; Du et al., 2018). Based on the economic conditions in rural areas, governments ought to encourage residents to choose high-maturity coals, natural gas, or electricity for heating and cooking.

### **Acknowledgments**

We appreciate Peter Hyde's comments and proofreading. This work was funded by the National Key R&D Program of China (2017YFC0212700), National Natural Science Foundation of China (41575116, 41622504, and 41805099), State Key Laboratory of Atmospheric Boundary Physics and Atmospheric Chemistry (LAPC-KF-2017-02), and the Hundred Talents Program in Zhejiang University. The data in this paper are available on Github at <https://github.com/liwjatmos/coalemission>.

---

## References :

- Adachi, K., & Buseck, P. R. (2011). Atmospheric tar balls from biomass burning in Mexico. *Journal of Geophysical Research*, *116*, D05204. <https://doi.org/10.1029/2010jd015102>
- Alexander, D. T. L., Crozier, P. A., & Anderson, J. R. (2008). Brown carbon spheres in East Asian outflow and their optical properties. *Science*, *321*(5890), 833-836. <https://doi.org/10.1126/science.1155296>
- Andreae, M. O., & Gelencsér, A. (2006). Black carbon or brown carbon? The nature of light-absorbing carbonaceous aerosols. *Atmospheric Chemistry and Physics*, *6*(10), 3131-3148. <https://doi.org/10.5194/acp-6-3131-2006>
- Bond, T. C., Covert, D. S., Kramlich, J. C., Larson, T. V., & Charlson, R. J. (2002). Primary particle emissions from residential coal burning: Optical properties and size distributions. *Journal of Geophysical Research*, *107*(D21), 8347. <https://doi.org/10.1029/2001jd000571>
- Bond, T. C., Streets, D. G., Yarber, K. F., Nelson, S. M., Woo, J. H., & Klimont, Z. (2004). A technology-based global inventory of black and organic carbon emissions from combustion. *Journal of Geophysical Research*, *109*, D14203. <https://doi.org/10.1029/2003jd003697>
- Cao, G. L., Zhang, X. Y., & Zheng, F. C. (2006). Inventory of black carbon and organic carbon emissions from China. *Atmospheric Environment*, *40*(34), 6516-6527. <https://doi.org/10.1016/j.atmosenv.2006.05.070>
- Chakrabarty, R. K., Moosmuller, H., Chen, L. W. A., Lewis, K., Arnott, W. P., Mazzoleni, C., et al. (2010). Brown carbon in tar balls from smoldering biomass combustion. *Atmospheric Chemistry and Physics*, *10*(13), 6363-6370. <https://doi.org/10.5194/acp-10-6363-2010>
- Chen, C. H., Wang, B. Y., Fu, Q. Y., Green, C., & Streets, D. G. (2006a). Reductions in emissions of local air pollutants and co-benefits of Chinese energy policy: a Shanghai case study. *Energy Policy*, *34*(6), 754-762. <https://doi.org/10.1016/j.enpol.2004.07.007>
- Chen, S. R., Xu, L., Zhang, Y. X., Chen, B., Wang, X. F., Zhang, X. Y., et al. (2017). Direct observations of organic aerosols in common wintertime hazes in North China: insights into direct emissions from Chinese residential stoves. *Atmospheric Chemistry and Physics*, *17*(2), 1259-1270. <https://doi.org/10.5194/acp-17-1259-2017>
- Chen, Y. J., Sheng, G. Y., Bi, X. H., Feng, Y. L., Mai, B. X., & Fu, J. M. (2005). Emission factors for carbonaceous particles and polycyclic aromatic hydrocarbons from residential coal combustion in China. *Environmental Science & Technology*, *39*(6), 1861-1867. <https://doi.org/10.1021/es0493650>
- Chen, Y. J., Zhi, G. R., Feng, Y. L., Fu, J. M., Feng, J. L., Sheng, G. Y., & Simoneit, B. R. T. (2006b). Measurements of emission factors for primary carbonaceous particles from residential raw-coal combustion in China. *Geophysical Research Letters*, *33*, L20815. <https://doi.org/10.1029/2006gl026966>
- Chen, Y. J., Zhi, G. R., Feng, Y. L., Liu, D. Y., Zhang, G., Li, J., et al. (2009). Measurements of Black and Organic Carbon Emission Factors for Household Coal Combustion in China: Implication for Emission Reduction. *Environmental Science & Technology*, *43*(24), 9495-9500. <https://doi.org/10.1021/es9021766>
- Chi, J. W., Li, W. J., Zhang, D. Z., Zhang, J. C., Lin, Y. T., Shen, X. J., et al. (2015). Sea salt aerosols as a reactive surface for inorganic and organic acidic gases in the Arctic troposphere. *Atmospheric Chemistry and Physics*, *15*(19), 11341-11353. <https://doi.org/10.5194/acp-15-11341-2015>
- Du, W., Li, X., Chen, Y., & Shen, G. (2018). Household air pollution and personal exposure to air pollutants in rural China - A review. *Environmental Pollution*, *237*, 625-638. <https://doi.org/10.1016/j.envpol.2018.02.054>
- EIA (2016). *International Energy Outlook 2016*, Washington, DC: U.S. Department of Energy.
- Ge, S., Xu, X., Chow, J. C., Watson, J., Sheng, Q., Liu, W. L., et al. (2004). Emissions of air pollutants from household stoves: Honeycomb coal versus coal cake. *Environmental Science & Technology*, *38*(17), 4612-4618.

---

<https://doi.org/10.1021/es049942k>

Gohlke, J. M., Thomas, R., Woodward, A., Campbell-Lendrum, D., Pruss-Ustun, A., Hales, S., & Portier, C. J. (2011). Estimating the Global Public Health Implications of Electricity and Coal Consumption. *Environmental Health Perspectives*, *119*(6), 821-826. <https://doi.org/10.1289/ehp.1002241>

Hand, J. L., Malm, W. C., Laskin, A., Day, D., Lee, T., Wang, C., et al. (2005). Optical, physical, and chemical properties of tar balls observed during the Yosemite Aerosol Characterization Study. *Journal of Geophysical Research*, *110*, D21210. <https://doi.org/10.1029/2004jd005728>

Hoffer, A., Tóth, A., Nyirő-Kósa, I., Pósfai, M., & Gelencsér, A. (2016). Light absorption properties of laboratory-generated tar ball particles. *Atmospheric Chemistry and Physics*, *16*(1), 239-246. <https://doi.org/10.5194/acp-16-239-2016>

Huang, R. J., Zhang, Y. L., Bozzetti, C., Ho, K. F., Cao, J. J., Han, Y. M., et al. (2014a). High secondary aerosol contribution to particulate pollution during haze events in China. *Nature*, *514*(7521), 218-222. <https://doi.org/10.1038/nature13774>

Huang, W., Bi, X., Zhang, G., Huang, B., Lin, Q., Wang, X., et al. (2014b). The chemical composition and stable carbon isotope characteristics of particulate matter from the residential honeycomb coal briquettes combustion (in Chinese). *Geochimica*, *43*(6), 640-646

Huang, W., Huang, B., Bi, X. H., Lin, Q. H., Liu, M., Ren, Z. F., et al. (2014c). Emission of PAHs, NPAHs and OPAHs from residential honeycomb coal briquette combustion. *Energy & Fuels*, *28*(1), 636-642. <https://doi.org/10.1021/ef401901d>

Jing, B., Tong, S. R., Liu, Q. F., Li, K., Wang, W. G., Zhang, Y. H., & Ge, M. F. (2016). Hygroscopic behavior of multicomponent organic aerosols and their internal mixtures with ammonium sulfate. *Atmospheric Chemistry and Physics*, *16*(6), 4101-4118. <https://doi.org/10.5194/acp-16-4101-2016>

Kong, S., Yan, Q., Zheng, H., Liu, H., Wang, W., Zheng, S., et al. (2018). Substantial reductions in ambient PAHs pollution and lives saved as a co-benefit of effective long-term PM<sub>2.5</sub> pollution controls. *Environment International*, *114*, 266-279. <https://doi.org/10.1016/j.envint.2018.03.002>

Kwieceńska, B., & Petersen, H. I. (2004). Graphite, semi-graphite, natural coke, and natural char classification - ICCP system. *International Journal of Coal Geology*, *57*(2), 99-116. <https://doi.org/10.1016/j.coal.2003.09.003>

Lacey, F. G., Henze, D. K., Lee, C. J., van Donkelaar, A., & Martin, R. V. (2017). Transient climate and ambient health impacts due to national solid fuel cookstove emissions. *Proceedings of the National Academy of Sciences of the United States of America*, *114*(6), 1269-1274. <https://doi.org/10.1073/pnas.1612430114>

Li, Q., Jiang, J. K., Wang, S. X., Rumchev, K., Mead-Hunter, R., Morawska, L., & Hao, J. M. (2017a). Impacts of household coal and biomass combustion on indoor and ambient air quality in China: Current status and implication. *Science of the Total Environment*, *576*, 347-361. <https://doi.org/10.1016/j.scitotenv.2016.10.080>

Li, W. J., Shi, Z. B., Zhang, D. Z., Zhang, X. Y., Li, P. R., Feng, Q. J., et al. (2012). Haze particles over a coal-burning region in the China Loess Plateau in winter: Three flight missions in December 2010. *Journal of Geophysical Research*, *117*, D12306. <https://doi.org/10.1029/2012jd017720>

Li, W. J., Shao, L. Y., Zhang, D. Z., Ro, C. U., Hu, M., Bi, X. H., et al. (2016). A review of single aerosol particle studies in the atmosphere of East Asia: morphology, mixing state, source, and heterogeneous reactions. *Journal of Cleaner Production*, *112*, 1330-1349. <https://doi.org/10.1016/j.jclepro.2015.04.050>

Li, W. J., Chi, J. W., Shi, Z. B., Wang, X. F., Chen, B., Wang, Y., et al. (2014). Composition and hygroscopicity of aerosol particles at Mt. Lu in South China: Implications for acid precipitation. *Atmospheric Environment*, *94*, 626-636. <https://doi.org/10.1016/j.atmosenv.2014.06.003>

Li, W. J., Xu, L., Liu, X. H., Zhang, J. C., Lin, Y. T., Yao, X. H., et al. (2017b). Air pollution-aerosol interactions produce more bioavailable iron for ocean ecosystems. *Science Advances*, *3*(3), 6.

---

<https://doi.org/10.1126/sciadv.1601749>

Li, X., Wu, J., Elser, M., Cao, J., Feng, T., El-Haddad, I., et al. (2018). Contributions of residential coal combustion to the air quality in Beijing-Tianjin-Hebei (BTH), China: A case study. *Atmospheric Chemistry and Physics*, 18(14), 10675-10691. <https://doi.org/10.5194/acp-18-10675-2018>

Lighty, J. S., Veranth, J. M., & Sarofim, A. F. (2000). Combustion aerosols: Factors governing their size and composition and implications to human health. *Journal of the Air & Waste Management Association*, 50(9), 1565-1618. <https://doi.org/10.1080/10473289.2000.10464197>

Liu, J., Mauzerall, D. L., Chen, Q., Zhang, Q., Song, Y., Peng, W., et al. (2016). Air pollutant emissions from Chinese households: A major and underappreciated ambient pollution source. *Proceedings of the National Academy of Sciences of the United States of America*, 113(28), 7756-7761.

<https://doi.org/10.1073/pnas.1604537113>

Liu, L., Kong, S. F., Zhang, Y. X., Wang, Y. Y., Xu, L., Yan, Q., et al. (2017). Morphology, composition, and mixing state of primary particles from combustion sources - crop residue, wood, and solid waste. *Scientific Reports*, 7, 5047. <https://doi.org/10.1038/s41598-017-05357-2>

Liu, W. X., Dou, H., Wei, Z. C., Chang, B., Qiu, W. X., Liu, Y., & Tao, S. (2009). Emission characteristics of polycyclic aromatic hydrocarbons from combustion of different residential coals in North China. *Science of the Total Environment*, 407(4), 1436-1446. <https://doi.org/10.1016/j.scitotenv.2008.10.055>

NBSC (2015). *China Energy Statistical Yearbook 2015*, Beijing: China Statistics Press.

NBSC (2016). *China Statistical Yearbook-2016*, Beijing: China Statistics Press.

Pósfai, M., Simonics, R., Li, J., Hobbs, P. V., & Buseck, P. R. (2003). Individual aerosol particles from biomass burning in southern Africa: 1. Compositions and size distributions of carbonaceous particles. *Journal of Geophysical Research*, 108(D13), 8483. <https://doi.org/10.1029/2002jd002291>

Pósfai, M., Gelencsér, A., Simonics, R., Arató, K., Li, J., Hobbs, P. V., & Buseck, P. R. (2004). Atmospheric tar balls: Particles from biomass and biofuel burning. *Journal of Geophysical Research*, 109, D06213.

<https://doi.org/10.1029/2003jd004169>

Reid, J. S., Koppmann, R., Eck, T. F., & Eleuterio, D. P. (2005). A review of biomass burning emissions part II: intensive physical properties of biomass burning particles. *Atmospheric Chemistry and Physics*, 5, 799-825.

<https://doi.org/10.5194/acp-5-799-2005>

Semeniuk, T. A., Wise, M. E., Martin, S. T., Russell, L. M., & Buseck, P. R. (2007). Hygroscopic behavior of aerosol particles from biomass fires using environmental transmission electron microscopy. *Journal of Atmospheric Chemistry*, 56(3), 259-273. <https://doi.org/10.1007/s10874-006-9055-5>

Shen, G. F., Yang, Y. F., Wang, W., Tao, S., Zhu, C., Min, Y. J., et al. (2010). Emission Factors of Particulate Matter and Elemental Carbon for Crop Residues and Coals Burned in Typical Household Stoves in China. *Environmental Science & Technology*, 44(18), 7157-7162. <https://doi.org/10.1021/es101313y>

Sun, J. X., Liu, L., Xu, L., Wang, Y. Y., Wu, Z. J., Hu, M., et al. (2018). Key Role of Nitrate in Phase Transitions of Urban Particles: Implications of Important Reactive Surfaces for Secondary Aerosol Formation. *Journal of Geophysical Research: Atmospheres*, 123(2), 1234-1243. <https://doi.org/10.1002/2017jd027264>

Sun, Y. L., Wang, Z. F., Fu, P. Q., Yang, T., Jiang, Q., Dong, H. B., et al. (2013). Aerosol composition, sources and processes during wintertime in Beijing, China. *Atmospheric Chemistry and Physics*, 13(9), 4577-4592. <https://doi.org/10.5194/acp-13-4577-2013>

Tóth, A., Hoffer, A., Nyirő-Kósa, I., Pósfai, M., & Gelencsér, A. (2014). Atmospheric tar balls: aged primary droplets from biomass burning? *Atmospheric Chemistry and Physics*, 14(13), 6669-6675.

<https://doi.org/10.5194/acp-14-6669-2014>

Wang, Y., Xu, Y., Chen, Y. J., Tian, C. G., Feng, Y. L., Chen, T., et al. (2016). Influence of different types of

---

coals and stoves on the emissions of parent and oxygenated PAHs from residential coal combustion in China. *Environmental Pollution*, 212, 1-8. <https://doi.org/10.1016/j.envpol.2016.01.041>

Zhang, C., He, X., Zhu, S., Wang, X., & Zhuang, H. (2011). *Distribution, Character and Utilization of Lignite in China*. Paper presented at 2011 Asia-Pacific Power and Energy Engineering Conference, IEEE, Wuhan.

Zhang, J., Liu, L., Wang, Y. Y., Ren, Y., Wang, X., Shi, Z. B., et al. (2017a). Chemical composition, source, and process of urban aerosols during winter haze formation in Northeast China. *Environmental Pollution*, 231, 357–366. <https://doi.org/10.1016/j.envpol.2017.07.102>

Zhang, J. J., & Smith, K. R. (2007). Household air pollution from coal and biomass fuels in China: Measurements, health impacts, and interventions. *Environmental Health Perspectives*, 115(6), 848-855. <https://doi.org/10.1289/ehp.9479>

Zhang, Y. X., Schauer, J. J., Zhang, Y. H., Zeng, L. M., Wei, Y. J., Liu, Y., & Shao, M. (2008). Characteristics of particulate carbon emissions from real-world Chinese coal combustion. *Environmental Science & Technology*, 42(14), 5068-5073. <https://doi.org/10.1021/es7022576>

Zhang, Z. Z., Wang, W. X., Cheng, M. M., Liu, S. J., Xu, J., He, Y. J., & Meng, F. (2017b). The contribution of residential coal combustion to PM<sub>2.5</sub> pollution over China's Beijing-Tianjin-Hebei region in winter. *Atmospheric Environment*, 159, 147-161. <https://doi.org/10.1016/j.atmosenv.2017.03.054>

Zhi, G. R., Chen, Y. J., Feng, Y. L., Xiong, S. C., Li, J., Zhang, G., et al. (2008). Emission characteristics of carbonaceous particles from various residential coal-stoves in China. *Environmental Science & Technology*, 42(9), 3310-3315. <https://doi.org/10.1021/es702247q>

Zhi, G. R., Zhang, Y. Y., Sun, J. Z., Cheng, M. M., Dang, H. Y., Liu, S. J., et al. (2017). Village energy survey reveals missing rural raw coal in northern China: Significance in science and policy. *Environmental Pollution*, 223, 705–712. <https://doi.org/10.1016/j.envpol.2017.02.009>

Zhou, W., Jiang, J. K., Duan, L., & Hao, J. M. (2016). Evolution of Submicrometer Organic Aerosols during a Complete Residential Coal Combustion Process. *Environmental Science & Technology*, 50(14), 7861-7869. <https://doi.org/10.1021/acs.est.6b00075>

Accepted Article

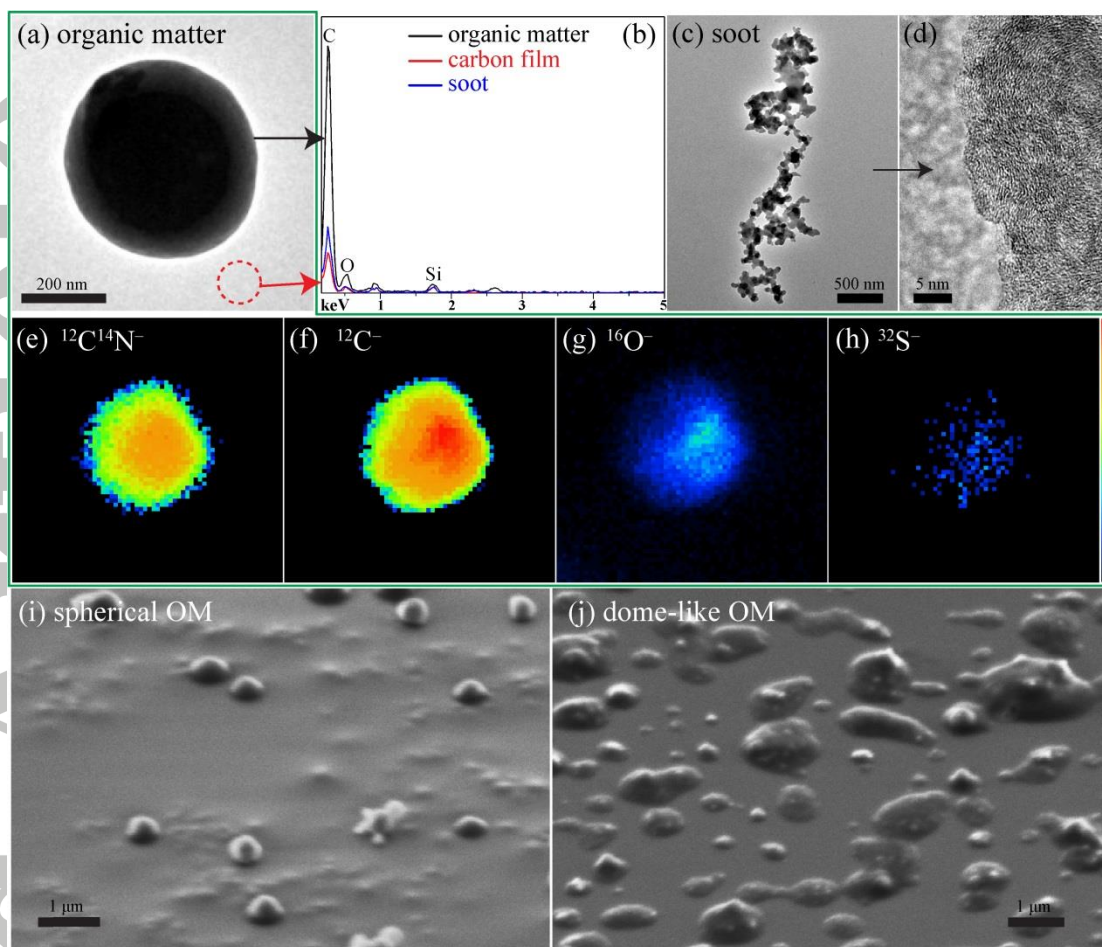


**Figure 1.** Microscopic chemical imaging of organic matter (OM) and soot emitted from residential coal burning. (a) Transmission electron microscopy (TEM) image of a typical spherical OM particle. (b) Energy-dispersive X-ray spectrometer (EDS) analyses of OM, carbon film, and soot. (c) TEM image of a soot particle. (d) High-resolution TEM image of soot containing the graphitic layers with onion-like structure. (e-h) NanoSIMS ion intensity of  $^{12}\text{C}^{14}\text{N}^-$ ,  $^{12}\text{C}^-$ ,  $^{16}\text{O}^-$ , and  $^{32}\text{S}^-$  in a spherical OM particle. (i-j) Scanning electron microscopy (SEM) images of spherical OM and dome-like OM taken with the sample stage tilted at a  $55^\circ$  angle.

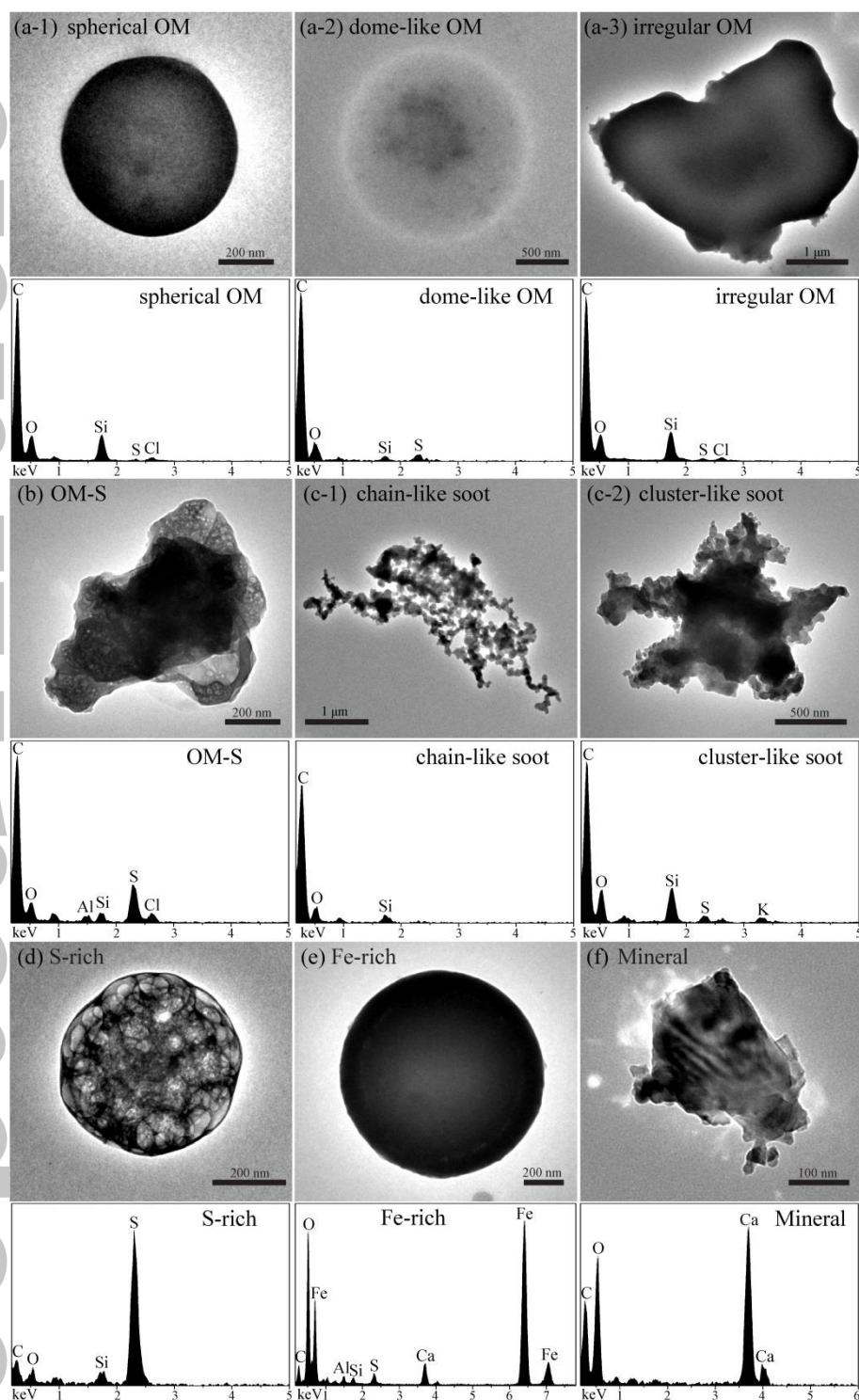


**Figure 2.** Transmission electron microscopy images and energy-dispersive X-ray spectrometer analyses of six types of primary particles from residential coal burning. (a) Organic matter (OM) particles including spherical OM (a-1), dome-like OM (a-2), and irregular OM (a-3). (b) OM-S particle containing minor Cl. (c) Soot particles including chain-like soot (c-1), and cluster-like soot (c-2). (d) Sulfur (S)-rich particle. (e) Iron (Fe)-rich metal particle. (f) Calcium (Ca)-rich mineral particle.

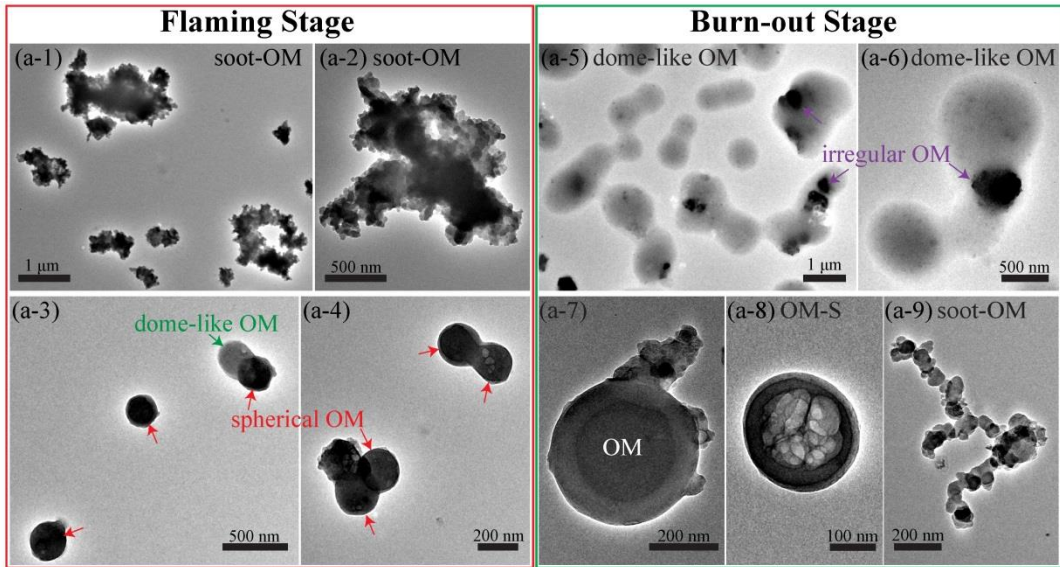


**Figure 3.** Transmission electron microscopy images of individual primary particles from residential lignite burning in the flaming and burn-out stages. The lignite was collected from Inner Mongolia (IM/LI). The red frame and the green frame indicate that primary particles were collected during the flaming stage and the burn-out stage, respectively.

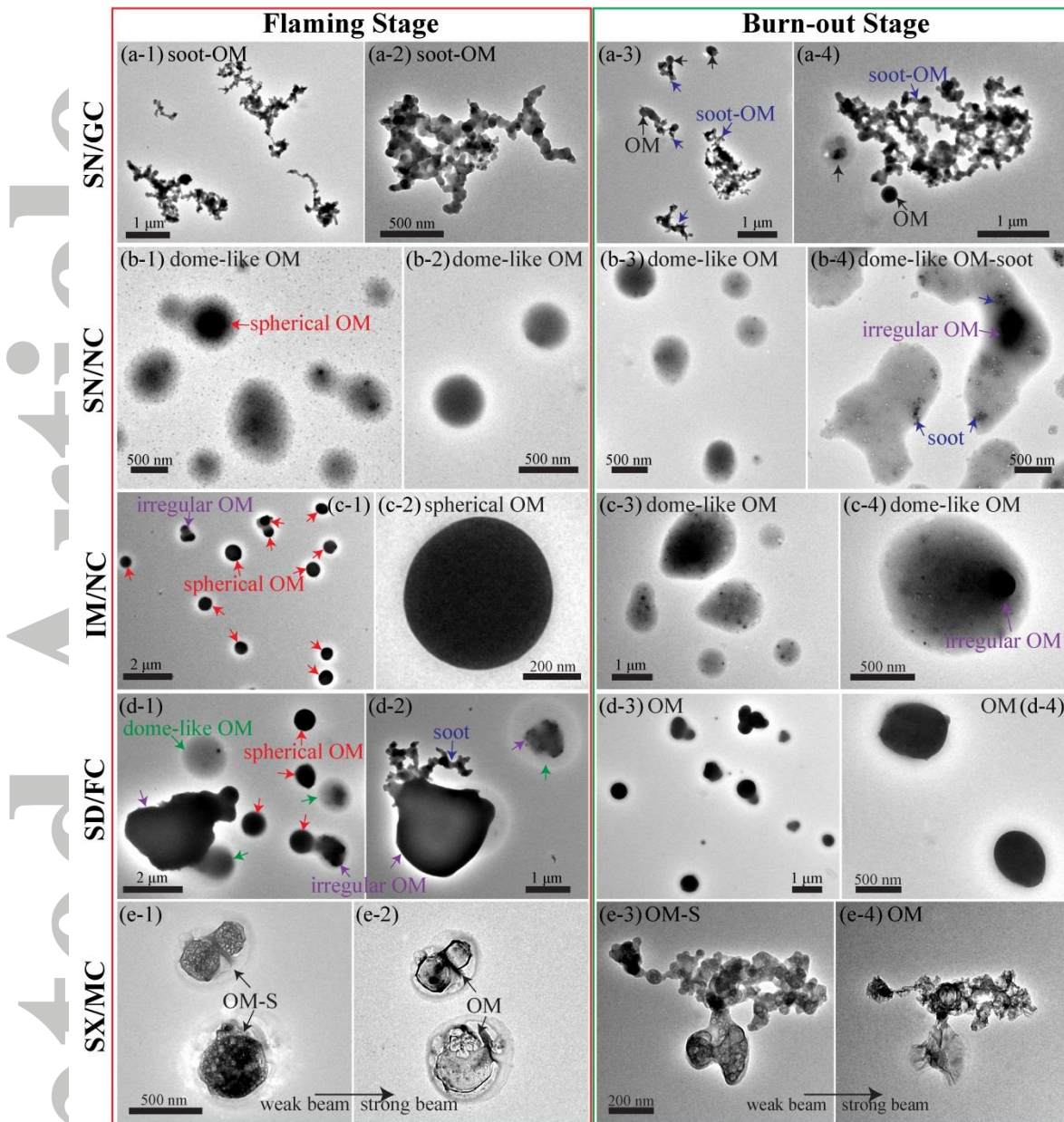


**Figure 4.** Transmission electron microscopy images of individual primary particles from residential bituminous coal burning in the flaming and burn-out stages. (a) Soot-organic matter (OM) and OM particles emitted from gas coal of Shaanxi (SN/GC). (b) OM particles emitted from non-caking coal of Shaanxi (SN/NC). (c) OM particles emitted from non-caking coal of Inner Mongolia (IM/NC). (d) OM and soot-OM particles emitted from fat coal of Shandong (SD/FC). (e) OM-S particles emitted from meager coal of Shanxi (SX/MC). The red frame and the green frame indicate that primary particles were collected during the flaming stage and the burn-out stage, respectively.

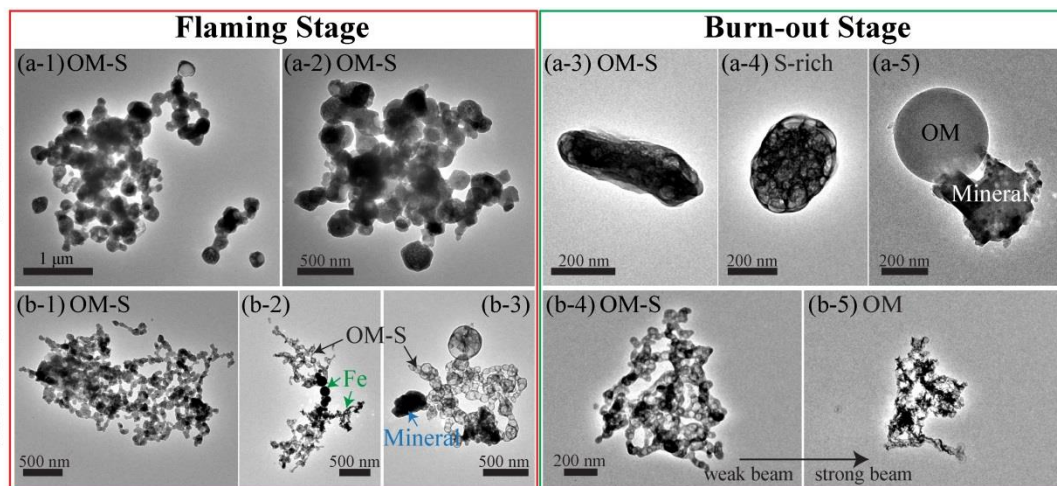


**Figure 5.** Transmission electron microscopy images of individual primary particles from residential anthracite and natural coke burning in the flaming and burn-out stages. (a) Organic matter (OM)-Sulfur (S), S-rich and mineral particles emitted from anthracite of Shanxi (SX/AN). (b) OM-S, metal and mineral particles emitted from natural coke of Shanxi (SX/NCC). The red frame and the green frame indicate that primary particles occurred in the flame stage and the burn-out stage, respectively.

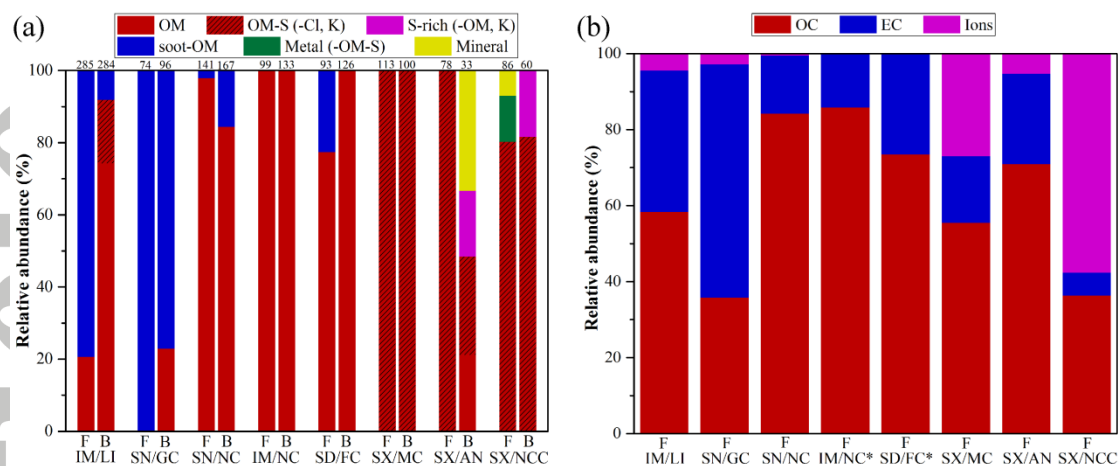


**Figure 6.** Component characteristics of fine primary particles from residential coal burning. (a) Individual particle analysis: relative abundances of six individual particle types from the flaming (F) and burn-out (B) stages of eight types of residential coal burning. (b) Bulk sample analysis: relative abundances of organic carbon (OC), elemental carbon (EC), and soluble inorganic ions in PM<sub>2.5</sub> from the flaming stage (F) of eight types of residential coal burning. Eight types of coal include lignite from Inner Mongolia (IM/LI), gas coal from Shaanxi (SN/GC), non-caking coal from Shaanxi (SN/NC), non-caking coal from Inner Mongolia (IM/NC), fat coal from Shandong (SD/FC), meager coal from Shanxi (SX/MC), anthracite from Shanxi (SX/AN), and natural coke from Shanxi (SX/NCC). Star (\*) indicates that soluble inorganic ions were not included.

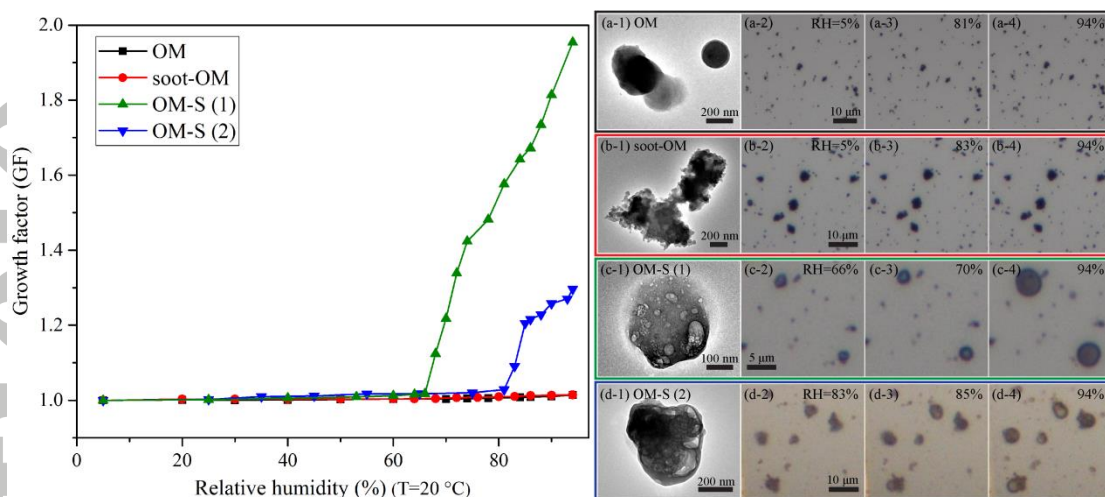


**Figure 7.** Hygroscopic growth of organic matter (OM), soot-OM, and OM-sulfur (S) particles emitted from residential coal burning as a function of relative humidity (RH). The left panel shows the growth factor (GF) of OM, soot-OM, OM-S (1) and OM-S (2) as a function of relative humidity (RH; when  $T = 20^{\circ}\text{C}$ ). The right panel shows transmission electron microscopy images of typical OM (a-1), soot-OM (b-1), and OM-S (c-1, d-1) particles in four samples and optical microscope images of the corresponding samples showing the variable shapes of OM (a-2/3/4), soot-OM (b-2/3/4) and OM-S (c-2/3/4, d-2/3/4) particles throughout a range of RH from 5% to 94%.

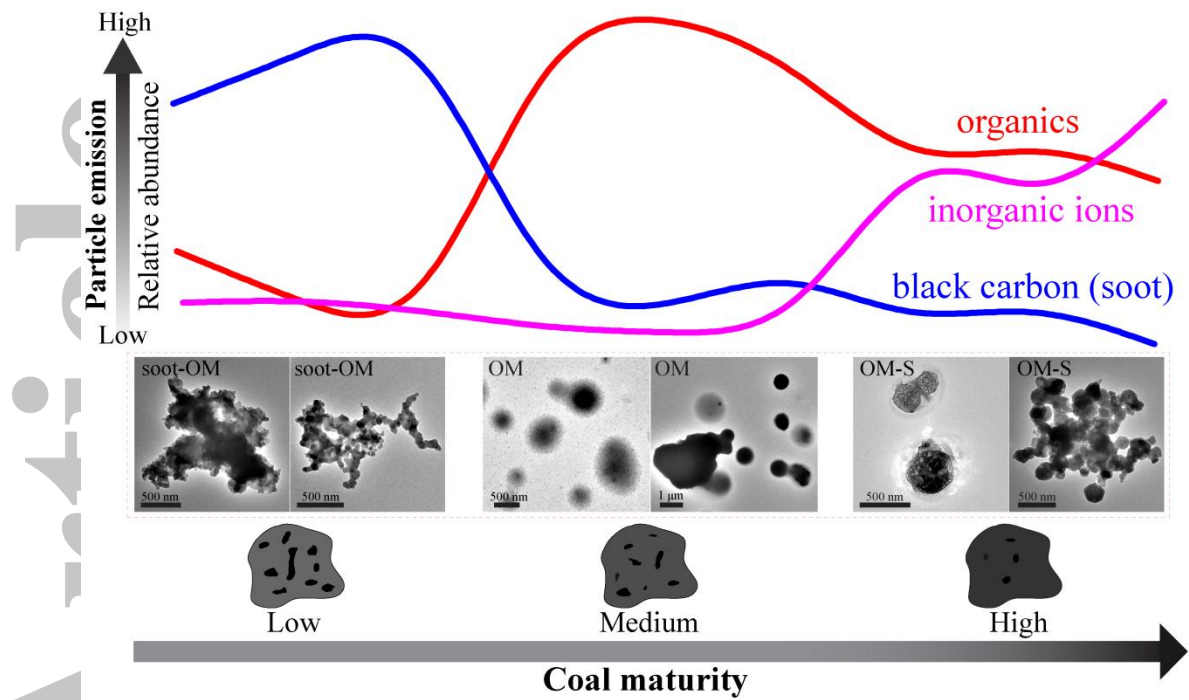


**Figure 8.** Schematic diagram showing the impacts of coal maturity on particulate properties in coal emissions during the flaming stage of residential coal burning.

**Table 1** *Information on Eight Types of Coal*

Production area	Types of coal	R <sub>o</sub> (%) <sup>a</sup>	Rank <sup>b</sup>	Coal ID
Inner Mongolia	Lignite	0.33	Lignite	IM/LI
Shaanxi	Gas coal	0.55	Bituminous coal	SN/GC
Shaanxi	Non-caking coal	0.58	Bituminous coal	SN/NC
Inner Mongolia	Non-caking coal	0.62	Bituminous coal	IM/NC
Shandong	Fat coal	0.94	Bituminous coal	SD/FC
Shanxi	Meager coal	1.98	Bituminous coal	SX/MC
Shanxi	Anthracite	2.03	Anthracite	SX/AN
Shanxi	Natural coke	7.38	Natural coke	SX/NCC

<sup>a</sup>Vitrinite reflectance of coal representing coal maturity. <sup>b</sup>Rank according to Chinese classification of coals (GB/T 5751-2009).

Accepted Article

**Table 2** Summary of Individual Primary Particles from the Flaming and Burn-out Stages of Eight Types of Coal.

Coal ID	Coal maturity	Stage	Particle classification	Number	Proportion (%)
IM/LI	Low maturity	Flaming	OM	59	21
			soot-OM	226	79
		Burn-out	OM	211	74
			OM-S	50	18
SN/GC	Low maturity	Flaming	soot-OM	74	100
		Burn-out	OM	22	23
			soot-OM	74	77
SN/NC	Medium maturity	Flaming	OM	138	98
			soot-OM	3	2
		Burn-out	OM	141	84
			OM-soot	26	16
IM/NC	Medium maturity	Flaming	OM	99	100
		Burn-out	OM	133	100
SD/FC	Medium maturity	Flaming	OM	72	77
			soot-OM	21	23
		Burn-out	OM	126	100
SX/MC	High maturity	Flaming	OM-S	113	100
		Burn-out	OM-S	100	100
SX/AN	High maturity	Flaming	OM-S	78	100
			Burn-out	OM	7
		OM-S		9	27
		S-rich		6	18
		Mineral	11	34	
SX/NCC	High maturity	Flaming	OM-S	69	80
			Metal-OM-S	11	13
			Mineral-OM-S	6	7
		Burn-out	OM-S	49	82
			S-rich	11	18